Emerging Electrical Properties of Graphene incorporated Photosynthetic Biofilms

Sanhita Ray,* Sayantani Sen,† Alakananda Das,‡ Anirban Bose,§ Anirban Bhattacharyya,¶ Avishek Das,** Sanatan Chattopadhyay,†† Hirak Patra,‡‡ Shib Shankar Singha,§§ Achintya Singha,¶¶ and Anjan Kr Dasgupta***

(Dated: April 29, 2017)

Biofilms have been a breeding ground for creation of novel biomaterials with emergent properties. We report immobilization of hydrophobic graphene by a growing photosynthetic biofilm. We obtained a conductive biomaterial that can form a Schottky diode when grown on a metallic electrode surface. Capacitive spectra on frequency axis were obtained for control biofilm, which showed isosbestic points at 0.9 and 6MHz when RMS voltage was changed. This implies a two state di-electric transition. Immobilization of graphene by biofilm shifts such electrical isosbestic points significantly. The additional implication of the present study is the emergence of voltage dependent conductance with conductance peaks near the Schottky diode threshold. The observed emergent properties may be helpful in biomaterial based design of sensors.

PACS numbers: 87.18.Fx,81.05.ue,85.30.Hi, 85.30.Kk

I. INTRODUCTION

Carbon nanomaterials (CNMs) present unique opportunities for application in electronic devices [1] due to their electron transport properties. Other than *in situ* growth [2] on device surfaces [3], it is difficult and costly to immobilize CNMs. Covalent modifications [4] often increase the defect density and impede electron conduction. Hence non-covalent functionalization [5] is the only way. Additionally, the high hydrophobicity [6] of CNMs prevents their dispersion in water.

Graphene is a two dimensional (2D) zero band gap CNM known for ballistic transport [7] of electrons. Its additional property of phonon conduction [8] is also known. Band gap of graphene may be modified by strain induction [9] wherein some curvature is introduced. A recent study has demonstrated use of *Bacillus subtilis* cell in wrinkling graphene sheet and consequent controlled anisotropy in conduction properties[10]. Graphene devices have been proposed as components of next generation advanced electronic or sensor devices [11–17].

We have aimed for a green immobilization of graphene by using biofilms- a process which may be adapted for a wider class of hydrophobic carbon nanomaterials (carbon nanotubes, fullerenes) as well as other 2-D materials. Our process utilizes whole living cells [18], hence targets a diminished carbon footprint. Cost is low since growing micro-organisms are used, instead of purified biomolecules like lipids [19].

Biofilms are well organized microbial aggregates that are known for their resilience to adverse environmental conditions like dehydration, shear stress and chemical agents. We have used the growth process of purple non-sulphur bacterial biofilm for graphene immobilization. Purple non-sulphur bacteria are capable of utilizing a wide variety of organic matter as nutrition source; at the same time it is photosynthetic and possesses light harvesting molecules [20] in its membrane, that act as electron carriers. They have atypical lipid molecules in their membranes, known as hopanoids [21], which increase membrane rigidity, and this may be important for withstanding the usual toxic effect of graphene on bacterial cells [22]. Conducting nanofibrils and capacitive elements i.e. cytochromes in bacterial (Geobacter) biofilms [23, 24] have been investigated recently and has opened up the the possibility of using microbes in electronic devices.

In most cases one attempts to use graphene as a negative regulator of biofilm growth[25]. This approach is closely related to a perception that biofilm corresponds to that formed by pathogenic bacteria. However if we consider biofilm of photosynthetic bacteria one may not be keen to suppress its growth. On the other hand there may be a beneficial exploitation such as Mccormick et al. [26, 27], if we can further the stabilization of such films as it may be useful as a photon capture or sensor device.

Some microbial and algal biofilms have been utilized for power generation in microbial fuel cells (MFCs). In situ reduced graphene oxide (RGO) incorporation has been used to modify microbial mat on MFC electrodes and increase its power output as well as in biophotovoltaic devices [27–31]. However these studies have used graphene oxide which disperses extremely well in water (indeed is commercially available as dispersions) as well as bacterial media, and biofilm induced bioreduction caused the RGO incorporation into biofilm. We, on the other hand, have used graphene powder, whose dispersion in water is poorer, and incorporation is by the stitching together such hydrophobic material

*Electronic address: daladysphinx@gmail.com
†Electronic address: sayantani163@gmail.com
‡Electronic address: adas4015@gmail.com
§Electronic address: 1989.anirban@gmail.com
¶Electronic address: anirban1@gmail.com
**Electronic address: avishek55das@gmail.com
††Electronic address: c_sanatan@yahoo.com
‡‡Electronic address: hirak.kumar.patra@liu.se
§§Electronic address: shibshankarsingha178@gmail.com
¶¶Electronic address: achintya@jcbose.ac.in
***Electronic address: adbioc@caluniv.ac.in;
University of Calcutta

by the biofilm. RGO, as a result of possessing higher defect density, interacts easily with a variety of purified bio-molecules (e.g. lipids [19, 32–38] and such immobilized systems have been utilized as sensor platforms.

Our initial investigations with this process found indications for Schottky diode formation [39]. The extensive flat surface of graphene prompted us to ask whether it would serve as substratum for biofilm growth. Alternatively, whether biofilm may act as a hydrophobic stitch device by incorporating graphene powder added to growth medium. The main questions being targeted are (a) how does immobilization by biofilm affect the electronic properties of graphene (b) how does graphene incorporation affect biofilm growth and functionality. This paper focuses primarily on interaction between the conduction behavior of graphene and reactive components of a living biofilm while presenting some results pertaining to purple non-sulphur biofilm growth in presence of graphene.

II. MATERIALS AND METHODS

A. Biocomposite synthesis

Bacterial strain used was *Rhodobacter capsulatus* SB1003 (RCSB), which is a purple non-sulphur bacterium, obtained as a gift from Dr. Patrick Hallenbach, University of Montreal. The growth medium used was yeast extract supplemented RCV medium (0.3 g/L yeast extract, 4 g/L malic Acid, 1 g/L ammonium chloride, 75 mg/L calcium Chloride, 1 mg/L nicotinic acid, 20 mg/L di-sodium EDTA, 120 mg magnesium chloride, 10 mM phosphate buffer at pH 6.8).

CVD synthesized graphene was provided by commercial manufacturers in powder form (Quantum Materials Corporation, Bangalore, AzoNano, UK).

Graphene was immobilized within biofilms by a one-pot method where the (IDEs) inter-digitated gold electrodes [40] , on glass were submerged in the bacterial media, graphene and inoculum was added to the same and anerobic growth was allowed to take place for 4 days, in presence of light (figures 1(a)-(g)). Graphene-biofilm composites grew as a continuous thick layer that extended over the metal electrodes as well as in the channel between two such electrodes, on the glass surface (insulator), see figure 1.

Graphene powder was directly added to culture medium inoculated with RCSB and biofilm growth was allowed to take place. Conditions for growth were: in transparent falcon tubes, kept up-right with no shaking, at room temperature and in presence of light. Bacterial growth with graphene was typically monitored for 4 days. For imaging purpose however biofilms grown for 11 days was taken. Please note that graphene powder was added to growth medium without any prior dispersion in organic solvents or acid. Control samples, without added graphene, were grown in identical conditions.

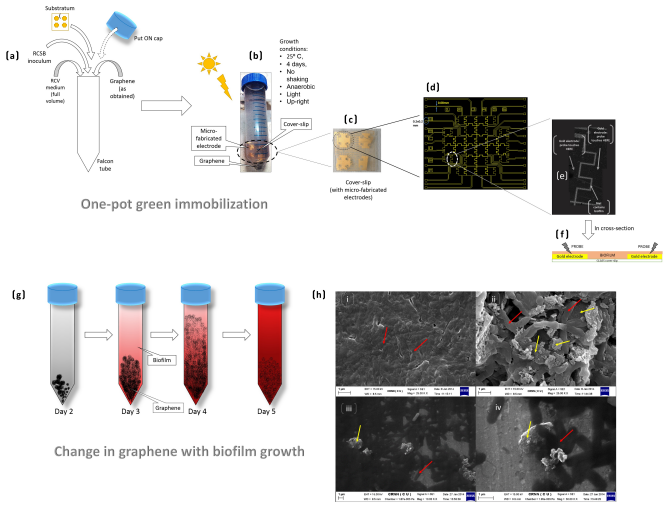

FIG. 1: Synthesis of graphene-biofilm bio-composite. (a) Schematic of components added to bacterial growth medium and conditions for growth of bio-composite. Panel (b) shows the set-up upon inoculation. Panel (c) shows gold electrodes fabricated upon glass coverslip, overall 4 complexes of electrodes are present one of which is shown in Panel (d) in schematic form. Each electrode complex consists of inter-digitated electrodes with a gap of 20 micron in between. (e) shows light microscopic image of micro-fabricated gold electrodes (dark area) on cover-slip with biofilm grown on top. Image obtained with lowest magnification of light microscope using 5X objective lenses, image is reconstructed from 3 overlapping micrographs of the electrode surface. The relatively lighter regions are the channels between electrodes containing no gold but with biofilm grown on the insulating substratum (glass). Panel (f) is a schematic of the same measurement set-up in cross-section.(g) Schematic of transformation of initially pristine graphene during biofilm growth(h)SEM images show graphene (yellow arrows) trapped by biofilm cells (red arrows) (ii) compared to micrographs of control samples (i) which do not show any such trapped structures, obtained after gold coating (upper row panels). (iii and iv) SEM images obtained before gold coating of fixed samples- bright patches are conducting graphene. Dark shadows are the non-conducting cells, bright background is conducting aluminum foil.

Graphene incorporated biofilm grew on the wall of the falcon tubes. Graphene was initially immiscible in the aqueous RCV medium and the black mass precipitated to the bottom of the falcon tube. With biofilm formation and secretion of surfactants (apparent from increased soapy frothing) over the course of 4 days of growth, the black mass became comparatively more dispersed in the medium. Biofilm formed with addition of graphene was blackish red and the black tint was most apparent at the bottom of the falcon tube, with film near the top of the tube being the least blackened (see figure 1 a,b and g).

Graphene incorporated biofilms were grown by adding 2 (g2), 3.3(g3), 4.4 (g4) and 5.5 mg of graphene to 50 ml media. Films were grown on bare glass cover-slips, inter-digitated gold electrodes (IDEs) on glass substrates or on aluminium foils by inserting them (see figure 1(c-f))

within the falcon tubes where biofilm growth was done. The cover-slip/foil/IDE remained completely immersed in the growth medium.

B. Scanning electron microscopy

SEM imaging: SEM images were obtained (see figure 1h)for samples grown on either bare cover-slips or aluminum foils wrapped on glass cover-slips. SEM images were obtained with scanning electron microscope (Model ZEISS EVO-MA 10) upgraded for imaging with biological samples. Images were obtained either with or without gold sputtering on top of either fixed or unfixed samples washed with milliQ water and dried at 50C overnight. Fixation was done with 2.5 % glutaraldehyde, washed, stained with 1 % osmium tetroxide, washed with milliQ then dehydrated in graded alcohol.

C. Raman spectroscopy

Raman spectrum of the graphene powder was obtained by dispersing the graphene powder in chloroform and casting a drop on quartz substrate. The Raman measurements were performed using a micro Raman set-up consisting of spectrometer (Lab RAM HR Jovin Yvon) and a Peltier cold CCD detector. An air cooled Argon-ion laser (Ar+) with a wavelength of 632 nm as an excitation light source. Laser was focused on the sample using 10X objective with a numerical aperture (NA) of 0.9. Power below 1 mW was used to avoid heating effect with 30 second integration time.

D. Biofilm formation assays

Biofilm formation on electrodes or cover-slip surfaces was confirmed by washing the IDEs (with biofilm grown on top) with distilled water and then observing them under light microscope. Figure 2(a) shows an IDE with control biofilm, i.e. without graphene. Figures 2 (b and c) respectivey represent the fully grown and and partially peeled biofilm layer in presence of graphene. Photographs were taken of the IDEs with biofilm grown on top (see Supplementary Figure S1)

Biofilm formation on the wall of each falcon tube was quantified by two methods.

- Pigment estimation: For pigment extraction, falcon tubes with biofilm grown on their walls was washed with milliQ to remove any adhering planktonic cells, followed by treatment with 1:4 solution of chloroform and ethanol, without disrupting the adhered biofilm. Whole volume of falcon tubes were filled with organic medium and closed tubes were kept at 50 C for 45 minutes. The organic extract was collected without disrupting attached biofilm. Absorption spectrum for each organic extract was measured in a spectrophotometer (Thermo Scientific , Model Evolution 300).

- Crystal violet staining [41]: Biofilm biomass was measured by first washing falcon tubes carefully to remove any adherent planktonic cells. After washing, whole falcon tubes were filled with 0.1% crystal violet in water, kept for 15 mins, then the staining solution was removed and washed with water to remove excess dye. The absorbed stain was extracted by treating the stained biofilms with 30% acetic acid, and the absorbance of this extract was measured at 595 nm.

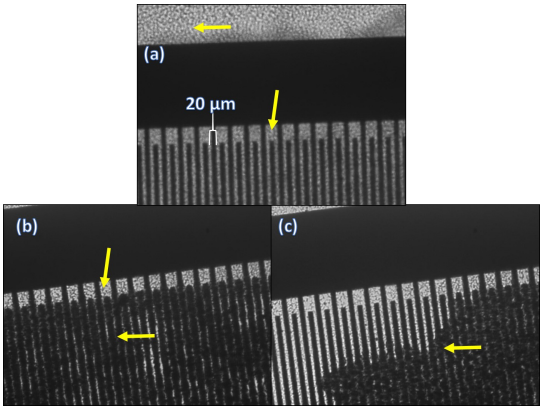

FIG. 2: Brightfield microscopic images at 20X (a) shows an IDE with control biofilm, i.e. without graphene. (finger width is 20 μm)(b) and c repectively represents the fully grown and and partially peeled biofilm with incorporated graphene. Yellow arrows mark the biofilm or graphene incorporated composite.

Control and graphene containing samples were grown and organic extract from biofilm adhered to falcon tube walls on 2nd, 3rd and 4th days of growth and absorbance at 370 nm was monitored.

E. Interdigitated electrode (IDEs) fabrication

Two independent sets of IDEs were used for measurement. The capacitance measurements were performed with IDE1 fabricated in our laboratory (gap=20 μm),and the I-V measurements were performed with IDE2 (gap=10 μm), commercially procured.

a. IDE1 fabrication Glass substrates were first cleaned using Trichloroethylene, Acetone, Isopropyl alcohol and deionized water. They were subsequently outgassed in a vacuum chamber at 120 C. Thin films of Chromium and Gold were successively deposited using resistive heating techniques. Electrodes with 20 m spacing were subsequently fabricated by standard photolithography and wet chemical etching processes using a solution of KI and iodine in water for gold and dilute HCl

for chromium. Cover-slips containing electrodes were further cleaned with isopropyl alcohol and sterilized with 70 % alcohol and air dried in laminar air flow. Biofilms were grown by immersing these cover-slips in bacterial media during growth. Device dimensions were: 3X2 digits, dimensions: 0.2 mm X 0.16 mm, gap=20 μm.

b. IDE2 A second set of interdigitated electrodes were purchased from commercial manufacturers Dropsens (IDEAU10) having cell constant=0.0118 cm-1, number of digits: 125 x 2, a digit length= 6.76 mm and gap 10 μm. This arrangement was important to achieve sufficient current for measurement [42].

F. Electrical measurements

Electrical characterizations, with DC (current-voltage measurements) and AC (capacitance measurements), were done by contacting gold probes (Probe Station, Cascade Microtech) onto two inter-digitated gold electrodes by piercing through the biofilm grown on top. Hence all measurements are for current flow across the channel((see figure 1 c,d,e and f). A two-probe system was used where one probe was earthed. The probes were connected to Keithley 4200-SCS Semiconductor Characterization System for performing measurements. For these measurements live biofilms (controls or containing graphene) were used. I-V curves were obtained by ramping voltage over various ranges and using various graphene biofilm stoichiometries. The following enlists the different conditions under which the electrical measurements were performed:

- All reading in log scale Figure (6)
- from -5 V to 5 V and back in quiet mode (IDE2, control biofilm, Figure (7)a)
- from -10 V to 10 V and back in quiet mode (IDE2, 2 mg graphene+biofilm, Figure (7)b)
- from -5 V to 5V and back in quiet mode (IDE2, 4.4 mg graphene+biofilm, Figure (7)c)
- from -1 V to 1 V and back in quiet mode (IDE2, 4.4 mg graphene+biofilm, Figure supplementary S5
- from -6V to 6 V and back in quiet mode (IDE2, 2 mg graphene+biofilm), Figure (see figure 7(b))

Quiet mode refers to instrumental settings that control data acquisition time. Fast or quite mode of data acquisition determines dV/dt which affects capacitive current and hysteretic properties.

Capacitance spectra, on frequency axis (range: from 10 KHz to 10 MHz), were measured using AC voltage. Bio-composite was found to be insensitive to any DC bias for these measurements. Root mean square (RMS) i.e. amplitude of the AC voltage was varied to obtain capacitance spectra modulation as a function of RMS voltage from 10 mV to 100 mV(instrumental limits).

III. RESULTS

A. Electron microscopy

SEM images of graphene containing bio-composites show wrinkled graphene (marked by yellow arrow in (see figure 1 (h) i-iv) trapped by biofilm cells (marked by red arrow in these figure panels). No trapped sheet-like structures may be observed in electron micro-graphs of control samples. The average diameter of as incorporated platelets was between 1-2 μm, with a wide size distribution. Some larger wrinkled sheet like structures were observed, trapped underneath cells. It is to be noted that these are 11th day samples, by which time cell sloughing has occurred to a great extent thus decreasing the surface area covered by cells. The platelets were confirmed as graphene by growing samples on aluminium foil and obtaining SEM images without gold coating. The conducting Al foil background showed up as a light color, the insulating bacterial cells as dark shadows and the highly conducting graphene as very bright patches. Micrographs could not be obtained for the dense control samples without gold coating, since the insulating samples got burned. Bacteria can be distinguished by their smoothness compared to rough surface of wrinkled graphene clusters.

a. Immobilization mechanism From the SEM images, the immobilization appears to be due to trapping of wrinkled graphene underneath biofilms and in between layers of biofilm cells. Purple non-sulphur biofilms adhere strongly to a large variety of surfaces [43] due to the presence of extra-cellular polysaccharides (EPS) and associated proteins. In addition, previous studies have shown incorporation of graphene into bacterial membranes, by hydrophobic interaction with phospholipid tails [22, 33]. The release of FlWG from clumps, as initially added, is probably due to surfactants released during biofilm formation [44]. Surfactants have been previously useful for obtaining single or few layered structures from multilayered 2D material [45].

B. Raman characterization

Raman spectrum was obtained for the graphene that was used for this study. Raman spectrum (figure 3) obtained with red laser (632 nm) showed $I_D : I_G$ ratio of 1.259 and using the relation of this ratio to average distance between defects (L_D) as in Cancado et al [46], L_D was determined to be 15.194 nm, which is greater than the average L_D for RGO which is around 3-4 nm [47, 48]. Hence our sample had relatively less defects compared to RGO and hence of higher hydrophobicity. Hydrophobicity is the important parameter that prevents interaction of graphene [49] with most aqueous based biosystems.

The anomalous hump like 2D peak has been reported for few layer wrinkled graphene [50] (FlWG), hence we may infer a part of the used graphene to contain FlWG.

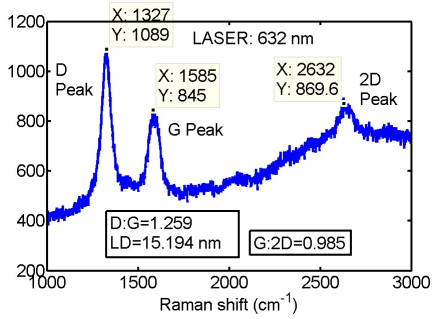

FIG. 3: Raman spectrum of the graphene used in these experiments, obtained with red laser (632 nm). $I_D : I_G$ ratio was 1.259, and corresponds to $L_D = 15.194$ nm. 2D peak obtained showed a hump. FWHM was much greater than is typical for monolayered graphene. These features have been previously described for few layered wrinkled graphene.

This is supported by the abnormally high FWHM of our samples of 65 cm^{-1} (G band) and 52 cm^{-1} (D band), as previously reported. In addition, the high intensity (almost same as I_G) around 2D region suggests decoration of wrinkled forms on the surface of larger sheets (since FlWG does not have as high 2D) and is supported by the SEM images of trapped sheets (supplementary figure S2). Raman spectra of used graphene is important since FlWG are known to possess an intrinsic band gap in many cases.

The wrinkled nature is supported by another Raman spectrum obtained with 488 nm laser, which shows an average distance between defect of 10 nm (see supplementary figure S3) yet distance between edges of 4.358 nm (according to Tunistra-Koenig relation). Wrinkling and folding may be responsible for reducing the size by bringing the edges much closer to each other and increasing the effective defect density. Please note that due to folding, sheet like structure is modified into platelets or particulate matter.

Raman spectra of biofilm incorporated graphene could not be obtained since Raman signal from carbohydrates (see supplementary figure S4) masked the Raman signature of graphene. This is proof that graphene was effectively trapped within extra-cellular polysaccharide, so that its surface is not accessible to light.

C. Biofilm formation assays

Addition of graphene has been shown to inhibit growth of bacteria in a number of studies [22, 25]. While growing the samples used earlier, we observed intenser pigmentation for graphene containing samples in our case.

Firstly, crystal violet staining of biofilms [41] was performed as described in Materials and Methods and amount of biofilm biomass per falcon tube was measured. Biomass increased with the addition of graphene in growth media, compared to control. This growth

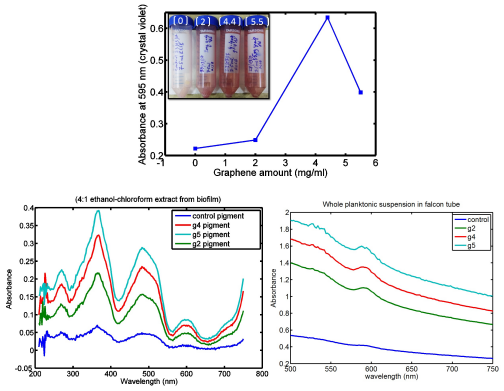

FIG. 4: (a) Variation in biofilm biomass with increasing graphene dose, estimated with crystal violet staining assay. Inset shows the biofilms adhered to falcon tube wall for each dose. (b) Variation in total pigment content of adhered biofilm determined by measuring the absorption spectra for organic extract from biofilms. (c) Absorption spectra of whole plantonic suspension for control and graphene incorporated samples.

promoting effect increased with increase in graphene dose. However for the highest dose (5.5 mg in 50 ml) biomass was lowered (see figure '4(a)). This probably indicates some sloughing off of films for the highest dose of graphene. The photograph in the inset shows the empty falcon tubes with biofilm grown on its walls. The numbers in brackets indicate quantity of graphene added to each falcon tube.

With respect to control, the total pigment content of biofilm on falcon tube walls increased with increasing graphene dose (see figure 4 (b)), for 4th day biofilms. This confirms increase of pigment content of biofilms when grown with graphene. Absorbance spectra of planktonic suspensions showed increasing O.D. with increasing graphene dose. This further confirms the growth promoting effects of graphene as well as indicating that there may be sloughing off from biofilm for the highest dose (5.5 mg).

The apparent growth promoting effect of graphene on RCSB biofilms was investigated by studying growth kinetics in presence and absense of graphene. From day 2 to day 4 of growth, absorbance at 370 nm showed a steeper increase (figure 5 a and b) when 2 mg of graphene was added, compared to control. This proves that graphene promotes Rhodobacter biofilm growth.

D. Electrical characterization

Our work shows the interaction between conducting graphene with charge carrier components in photosynthetic biofilms. IDE2 was used for current voltage measurements. IDE1 was used for capacitance measurements.

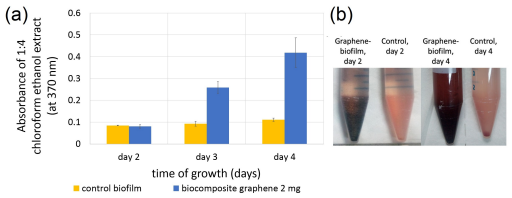

FIG. 5: Total pigment of biofilm over 4 days (a) Change in pigment content of graphene-biofilm composite compared to Rhodobacter biofilm over 2-4 days of growth. Estimation of pigment is given by absorbance at 370 nm of organic extract (chloroform: ethanol= 1: 4) of composite/control films, which corresponds to peak shown by organic extract. (b) Shows photographs of control and biocomposite after growth of days 2 and 4. For both (a) and (b) 2 mg graphene was added to 15 ml falcon tube filled with media. Triplicate sets of control and graphene containing composites were used for results in left panel.

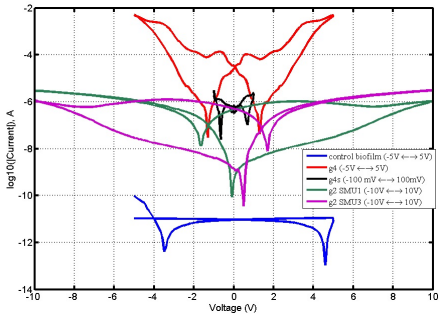

FIG. 6: Current voltage measurements for graphene containing (g2 and g4) and control sample. Graph shows log_{10} of absolute values of current as obtained during a single loop from negative to positive voltage and back. The black loop represent data for g4 when voltage range was smaller (-1 to 1V and back). Current voltage measurements were performed with graphene biofilm composites grown on IDE2. For errorbars see figure 7(a-c).

1. *IV curves*

Graphene incorporation into biofilm resulted in increased current flow, of the order of 10^{-3} A, for graphene dose of 4.4 mg in 50 ml (g4, see figure 6), compared to control, which gave current of the order of $10^{-}11$ A (see figure 6). For graphene dose of 2 mg in 50 ml (g2, see figure 6), current was of the order of 10^{-6} A, thus demonstrating that current through the biofilm depended on the quantity of graphene added to growth media. This proves graphene incorporation into biofilm.

Graphene incorporated biofilms exhibited a threshold (TH) in current conduction; no such threshold was present in control biofilm (see 7 (a-c)). Threshold may be taken to be a critical voltage above which current conduction is allowed. Presence of threshold indicates formation of a Schottky diode like junction [51] between biocomposite and the two gold electrodes. Since graphene is the

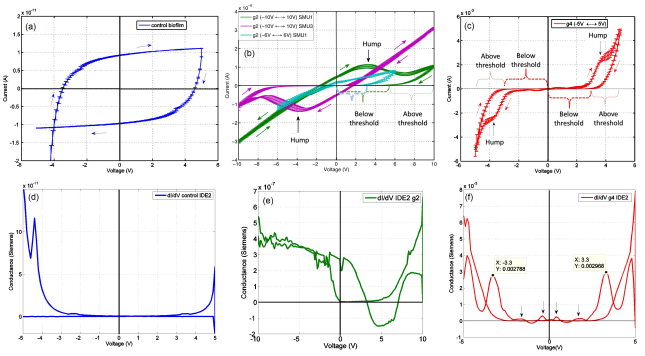

FIG. 7: (a) IV curve for control biofilm showing hysteretic properties (area within the curve) of the biomaterial. (b) IV curve for biofilm-graphene composite grown with 2 mg graphene in 50 ml media (g2). Green and purple curves are for same sample but SMUs were interchanged. (c) IV curve for biofilm-graphene composite grown with 2 mg graphene in 50 ml media (g4). For (a-c) arrows indicate up or down sweep of voltage in each case. (d-f) Voltage dependent conductance derived from (dI/dV) at a given V for control biofilm, g2 and g4, respectively. The arrows in (f) show smaller conductance peaks along with the prominent peak at $|V| = 3.3V$, dI/dV were for obtained using mean current values.

major conductive element in the biocomposite, we may conclude emergence of band gap in biofilm incorporated graphene. The results regarding Schottky threshold are summarized in Table **??**.

For g4 (see 7 (c)), the Schottky threshold was symmetric (STH) with forward(F, V > 0) and reverse bias(R, V<0). Sharp rise in current conduction occured for $|V|$ > 3.2 V, in both cases.

However typical Schottky barrier was observed only when $|V|$ was decreased from higher to lower values (i.e. voltage step-down followed the inequality $d|V|/dt < 0$). On the contrary if we follow the inequality $d|V|/dt > 0$ a hump in current conduction was observed (see Figure 7 b,c,e and f) near the Schottky threshold. Associated hysteresis in the IV curve (area within the curve) may be noted.

The gradient of current with respect to voltage (dI/dV, see Figure 7 (f)) i.e. point-to-point conductance showed sharp peaks at $\pm 3.3V$. Smaller peaks were observed at 0.4 and 1.6 V. The hump in current voltage curve correspond to the anomalous conductance peaks at $|V|$=3.3 V. Voltage dependent conductance peaks [52] are important since they may be an indication of ballistic transport, in this case occuring at room temperature ($T >> 77K$) .

When measurements were performed over smaller voltage range -1 to 1 V (g4s, see figure 6, supplementary figure S5), for g4, similar current-voltage curve was obtained as compared to -5 to 5 V, but no threshold was demonstrated. A scaling behavior of the I-V pattern in the 2 ranges (-1 to 1 V and -5 to 5 V, see figure 6) was observed.

For g2, threshold was assymetric (ATH, see Figure 7 (b)) and present only in case of forward bias (for green

TABLE I: Different thresholds and conductance emerging at varying stoichiometry of graphene and biofilm - experiments at different voltage ranges

Graphene →[a]	0	2	4.4
V-Range ↓			
-10-10V	ND[b]	AT[c](6V)dI/dV <0	ND
-5-5V	NT[d], $\frac{dI}{dV} > 0$	AT(2.5V) $\frac{dI}{dV} < 0$	ST[e](6V), $\frac{dI}{dV} > 0$
-1-1	ND	ND	NT

[a]Mg per 50 ml of medium
[b]Not Done
[c]Asymmetric Threshold
[d]No Threshold
[e]Symmetric Threshold

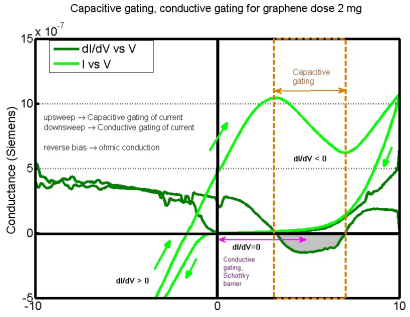

FIG. 8: Current voltage curve for g2, overlayed with dI/dV versus voltage. Shows conductive gating and capacitive gating. Mean values of current were used.

line). Measurement with reverse bias showed ohmic conduction (for green line). Thus one way Schottky diode was formed. This was confirmed by inverting the source measure units (SMU1 and SMU3) (see Figure 7 (b), purple line), which gave an inverted IV curve. This assymetry was obtained only when low graphene dose was used (compare with Figure 7(c)).

For g2, similar to g4, only voltage step-down ($d|V|/dt < 0$) resulted in Schottky barrier (conductive gating, dI/dV = 0,). For voltage step-up ($d|V|/dt > 0$), capacitive gating was exhibited over a voltage range of 3.3 V to 7 V. By capacitive gating we refer to decrease in current with increase in voltage (dI/dV < 0, see Figure 8). Measurement with smaller voltage range for g2 (g2s) resulted in shifted Schottky threshold along with disappearence of capacitive gating (blue line see Figure 7 (b)).

The conductance (dI/dV) versus voltage curve (see Figure 7(e), 8) for g2 shows this gate associated with negative conductance. Negative dI/dV implies flow of current opposite to the applied voltage implying emergence of capacitive component (see supplementary Figure S6). Area under the curve for this negative conductance region would give magnitude of capacitive current (see shaded area of figure 8). In figure 8, two regions are marked as conductive and capacitive gating. The regions show gates beyond wich current rises steeply.

2. *Capacitance profiles*

Capacitance profiles of both control (figure 9 (a)) and graphene incorporated biofilms (figure 9 (b-d)) exhibited co-dependence on frequency (ν) and RMS of AC voltage used for capacitance determination. Transition points were obtained such that capacitance values increased on one side (blue arrows) and decreased (red arrows) on other side of a particular frequency, upon RMS voltage variation. Spectra show an approximate convergent behavior near these transition points, i.e. values of capacitance come very close to each other and RMS dependence becomes negligible. We refer to these characteristic frequencies as capacitive isosbestics points, along the same line as spectrophotometric isosbestic points [54]. Isosbestic points may be interpreted as signifying a two-state dielectric transition, A → B, in response to changing AC voltage amplitude. Isosbestic point is important in the present context because the media being studied are complex dielectrics, yet isosbestic points provide a specific benchmark for characterization and detection.

For control biofilms (figure 9 (a)), isosbestic points were located at 0.9 and 6 MHz. Increased RMS voltage resulted in increased capacitance at 0.9 MHz $< \nu <$ 6MHz (peak response at 5 MHz) with concomitant decrease for $\nu < 0.9MHz$ and $\nu > 6MHz$ (peak response at 80 KHz and 9 MHz). Graphene incorporated biofilms demonstrated changes in both isosbestic points, with the frequencies corresponding to isosbestic points exhibiting unusually high standard deviation of capacitance values for RMS=10 mV. The frequency at which peak response occured i.e. 5 MHz showed a clear shift to 4 MHz for higher graphene doses (3.3 and 4.4 mg), see yellow circle in Figure 9 (a-d). It should be noted that with increasing RMS, bandpass properties of the dielectric changes and it transitions into an all-pass dielectric. We may translate the converging behavior into a frequency gate.

We explain the capacitive isosbestic point as occuring due to dipole alignment sensitivity to amplitude of sinusoidally varying voltage. Increasing RMS voltage resulted in increasing capacitance at < 6 MHz (peak response at 5 MHz) and decreasing capacitance at > 6 MHz (peak response at 9 MHz). This signifies that overall there are 2 dielectric states of the material (say P, Q) each of which show maximum alignment to the right and left of 6 MHz respectively. Increasing the RMS voltage converts P → Q. At 6 MHz, decrease in alignment of one state is exactly compensated for by increase in alignment of the other state. Depending upon whether it is a mole-to-mole P → Q conversion, unique isosbestic point is obtained, otherwise points of intersection shift.

A shifting convergence point signifies the generation of inter-mediates [54], during transition from one state to another. Addition of higher quantities of graphene may contribute towards generation of dielectric intermediates e.g. by adsorption of photosynthetic pigments. The high standard deviation of capacitance (at RMS=10 mV), selectively in the transition zone, strongly points towards

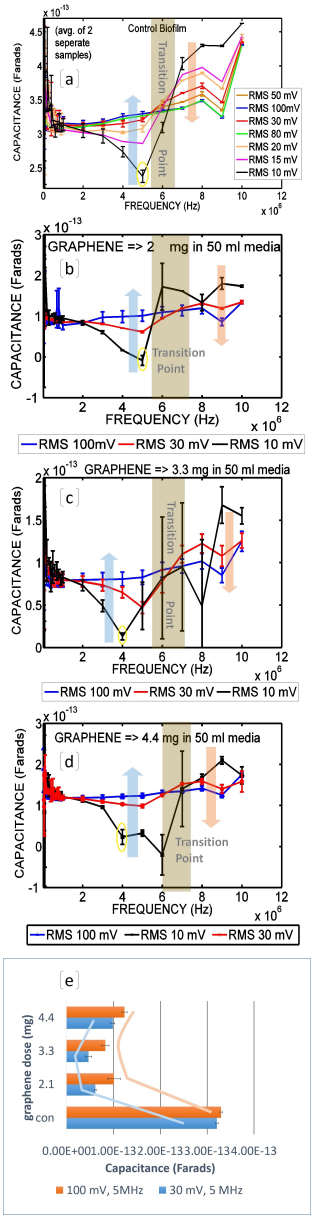

FIG. 9: (a) Capacitance profiles of control biofilm.A transition point was obtained (marked by a grey zone in figure) such that capacitance increased with RMS (from 10 to 100 mV) on one side (blue arrow) and decreased with RMS on the other side (orange arrow). (b-d) Capacitance spectra of bio-composites (at RMS voltages: 10, 30 and 100 mV) for different amounts of graphene (2, 3.3 and 4.4 mg) added to 50 ml media. Standard deviations were observed to be abnormally high for lowest RMS =10 mV, selectively around the transition zone, only for the graphene containing samples. Frequency of highest response (yellow circle, at RMS=10 mV), shifted. (e) Dependence of capacitance (at 30 and 100 mV, and 5MHz) on graphene dose. The pale blue and pale orange lines are hand-drawn guides for the eye, showing the overall trend. Values of capacitance are given for device specifications: 3 fingers, dimensions: 0.2 mm X 0.16 mm, gap=20 μm

role of graphene in affecting dipolar rearrangement in its vicinity.

Graphene incorporation during biofilm growth resulted in overall decreased (figure 9 (e)) capacitance, compared with control biofilm. This indicates that there is formation of spanning clusters of conducting graphene between gold electrodes resulting in a discharge current, thus dissipating the charge stored. This is consistent with the increased current flow with DC voltage. For lower doses of graphene added (2 mg and 3.3 mg), capacitance decreased. For 4.4 mg graphene, the trend reversed and capacitance increased, compared to lower doses (still lower than control). Figure 9 (e) shows this dose dependence for 30 and 100 mV. Increase in capacitance value for 4.4 mg graphene, suggests (a) increase in charge storing molecules when biofilm growth occurs in presence of graphene. This was supported by the pigment estimation from biofilms of the different samples (see figures 4(b) and 5(a)) (b) increased di-electric alignment in the vicinity of graphene caused by stacking interaction with planar dipoles.

IV. DISCUSSIONS

a. Origin of the Schottky threshold Presence of Schottky barrier points to presence of band gap in entrapped graphene. Change in nature of threshold for different graphene-biofilm stoichiometries points to modulation of the band gap by biofilm.

Graphene is a zero-band gap material meaning that there is no energy gap between its valence and conduction bands. Hence at room temperature bare graphene behaves as a metal. However, band gap is generated with strain induction in graphene or upon [9] functionalization. Few layer wrinkled graphene is known to exhibit band gap [50]. We explain the Schottky diode-like behavior as emerging due to (a) non-covalent functionalization of graphene by induction into lipid membranes of bacterial cells, due to hydrophobic interaction (b) graphene being held in a strained configuration due to trapping [55] by extra-cellular polysaccharide (c) the intrinsic band gap of FlWG modified by the above two processes.

All of the above processes induce curvature in otherwise flat graphene monolayer [10]. Introduction of curvature is associated with generation of chiral vector. This curvature is analogous to the curvature in case of carbon nanotubes. Curvature in CNTs is described by its chiral vector. The chiral vector in carbon nanotubes is given by,

$$\hat{C}_h = n\hat{a}_1 + m\hat{a}_2 \tag{1}$$

where, n and m are integers and $\hat{a}_1$ and $\hat{a} + 2$ are the unit vectors of the carbon nano-lattice. In terms of the integers (n,m), the nanotube diameter d_t and the chiral angle which govern their electrical properties are given

by[56, 57]:

$$d_t = \frac{\sqrt{3}a_{C-C}\sqrt{m^2+mn+n^2}}{\pi} \quad (2)$$

$$\theta = \tan^{-1}\left(\frac{\sqrt{3}\,n}{2m+n}\right) \quad (3)$$

It follows that carbon nanotube is metallic when n = m, semi-metallic when n-m=3i semiconducting when n-m$\neq$ 3i i being an integer. Thus chiral vectors affect band gap.

Hence our next hypothesis from this work is that graphene-to-bacteria stoichiometry (compare figures 7 (b) and (c)) controls the nature of curvature (represented by chiral vectors) and hence the emergent band gap of trapped graphene. This would explain the difference in nature of Schottky barrier for the two doses of graphene.

V. CONCLUSIONS

Emerging electrical property as a result of interaction between biofilm and graphene is reported. Biofilm has been shown to be an effective modulator of Schottky junction formation on metal electrode surface. Emergence of threshold was found to depend on graphene-biofilm stoichiometries. Voltage dependent conductance peaks were observed for higher graphene containing samples. A frequency gate occured, as revealed by isosbestic patterns, in capacitance spectrum on frequency axis, upon varying amplitude of AC input. Thus charge carrying capacity of 2D graphene composite becomes tunable and the device becomes a switchable capacitor. Raman spectra reveal the comparative (with respect to RGO) lower defect in wrinkled graphene nanoplatelet, proving that biofilm is a cheap hydrophilic platform for immobilizing hydrophobic graphene.

Acknowledgments

This work was supported by DBT (BT/PR3957/NNT/28/659/2013). SR thanks CSIR-India for Senior Research Fellowship (Sanction no.: 09/(028)0875).

[1] S. J. Tans, A. R. Verschueren, C. Dekker, Room-temperature transistor based on a single carbon nanotube, Nature 393 (6680) (1998) 49-52.
[2] G. Lippert, J. Dabrowski, Y. Yamamoto, F. Herziger, J. Maultzsch, M. C. Lemme, W. Mehr, G. Lupina, Molecular beam growth of micrometer-size graphene on mica, Carbon 52 (2013) 40–48.
[3] N. R. Franklin, Q. Wang, T. W. Tombler, A. Javey, M. Shim, H. Dai, Integration of suspended carbon nanotube arrays into electronic devices and electromechanical systems, Applied Physics Letters 81 (5) (2002) 913–915.
[4] J. Zhao, H. Park, J. Han, J. P. Lu, Electronic properties of carbon nanotubes with covalent sidewall functionalization, The Journal of Physical Chemistry B 108 (14) (2004) 4227–4230.
[5] R. J. Chen, S. Bangsaruntip, K. A. Drouvalakis, N. W. S. Kam, M. Shim, Y. Li, W. Kim, P. J. Utz, H. Dai, Noncovalent functionalization of carbon nanotubes for highly specific electronic biosensors, Proceedings of the National Academy of Sciences 100 (9) (2003) 4984–4989.
[6] S. Li, H. Li, X. Wang, Y. Song, Y. Liu, L. Jiang, D. Zhu, Super-hydrophobicity of large-area honeycomb-like aligned carbon nanotubes, The journal of physical chemistry B 106 (36) (2002) 9274–9276.
[7] P. Rickhaus, M.-H. Liu, P. Makk, R. Maurand, S. Hess, S. Zihlmann, M. Weiss, K. Richter, C. Schönenberger, Guiding of electrons in a few mode ballistic graphene channel, Nano letters.
[8] J. H. Seol, I. Jo, A. L. Moore, L. Lindsay, Z. H. Aitken, M. T. Pettes, X. Li, Z. Yao, R. Huang, D. Broido, et al., Two-dimensional phonon transport in supported graphene, Science 328 (5975) (2010) 213–216.
[9] M. Y. Han, B. Ozyilmaz, Y. Zhang, P. Kim, Energy band-gap engineering of graphene nanoribbons, Physical review letters 98 (20) (2007) 206805.
[10] S. Deng, E. Gao, Y. Wang, S. Sen, S. T. Sreenivasan, S. Behura, P. Král, Z. Xu, V. Berry, Confined, oriented, and electrically anisotropic graphene wrinkles on bacteria, ACS nano 10 (9) (2016) 8403–8412.
[11] Q. Zhou, A. Zettl, Electrostatic graphene loudspeaker, Applied Physics Letters 102 (22) (2013) 223109.
[12] P. K. Ang, W. Chen, A. T. S. Wee, K. P. Loh, Solution-gated epitaxial graphene as ph sensor, Journal of the American Chemical Society 130 (44) (2008) 14392–14393.
[13] S.-R. Guo, J. Lin, M. Penchev, E. Yengel, M. Ghazinejad, C. S. Ozkan, M. Ozkan, Label free dna detection using large area graphene based field effect transistor biosensors, Journal of nanoscience and nanotechnology 11 (6) (2011) 5258–5263.
[14] P. Li, B. Zhang, T. Cui, Towards intrinsic graphene biosensor: A label-free, suspended single crystalline graphene sensor for multiplex lung cancer tumor markers detection, Biosensors and Bioelectronics 72 (2015) 168–174.
[15] T. Liu, H. Su, X. Qu, P. Ju, L. Cui, S. Ai, Acetylcholinesterase biosensor based on 3-carboxyphenylboronic acid/reduced graphene oxide–gold nanocomposites modified electrode for amperometric detection of organophosphorus and carbamate pesticides, Sensors and actuators B: Chemical 160 (1) (2011) 1255–1261.

[16] O. Parlak, A. Tiwari, A. P. Turner, A. Tiwari, Template-directed hierarchical self-assembly of graphene based hybrid structure for electrochemical biosensing, Biosensors and Bioelectronics 49 (2013) 53–62.

[17] M. A. Nigro, G. Faggio, F. Fedi, T. Polichetti, M. L. Miglietta, E. Massera, G. Di Francia, F. Ricciardella, Cross interference effects between water and nh 3 on a sensor based on graphene/silicon schottky diode, in: AISEM Annual Conference, 2015 XVIII, IEEE, 2015, pp. 1–4.

[18] A. Y. Chen, Z. Deng, A. N. Billings, U. O. Seker, M. Y. Lu, R. J. Citorik, B. Zakeri, T. K. Lu, Synthesis and patterning of tunable multiscale materials with engineered cells, Nature materials 13 (5) (2014) 515–523.

[19] T. Bhattacharyya, A. K. Dasgupta, N. R. Ray, S. Sarkar, Molecular discriminators using single wall carbon nanotubes, Nanotechnology 23 (38) (2012) 385304.

[20] B. A. Diner, V. Petrouleas, J. J. Wendoloski, The iron-quinone electron-acceptor complex of photosystem ii, Physiologia Plantarum 81 (3) (1991) 423–436.

[21] T. Rezanka, L. Siristova, K. Melzoch, K. Sigler, Hopanoids in bacteria and cyanobacteria-their role in cellular biochemistry and physiology, analysis and occurrence, Mini-Reviews in Organic Chemistry 7 (4) (2010) 300–313.

[22] Y. Tu, M. Lv, P. Xiu, T. Huynh, M. Zhang, M. Castelli, Z. Liu, Q. Huang, C. Fan, H. Fang, et al., Destructive extraction of phospholipids from escherichia coli membranes by graphene nanosheets, Nature nanotechnology 8 (8) (2013) 594–601.

[23] G. Reguera, K. P. Nevin, J. S. Nicoll, S. F. Covalla, T. L. Woodard, D. R. Lovley, Biofilm and nanowire production leads to increased current in geobacter sulfurreducens fuel cells, Applied and environmental microbiology 72 (11) (2006) 7345–7348.

[24] N. S. Malvankar, T. Mester, M. T. Tuominen, D. R. Lovley, Supercapacitors based on c-type cytochromes using conductive nanostructured networks of living bacteria, ChemPhysChem 13 (2) (2012) 463–468.

[25] W. Hu, C. Peng, W. Luo, M. Lv, X. Li, D. Li, Q. Huang, C. Fan, Graphene-based antibacterial paper, ACS nano 4 (7) (2010) 4317–4323.

[26] A. J. McCormick, P. Bombelli, A. M. Scott, A. J. Philips, A. G. Smith, A. C. Fisher, C. J. Howe, Photosynthetic biofilms in pure culture harness solar energy in a mediatorless bio-photovoltaic cell (bpv) system, Energy & Environmental Science 4 (11) (2011) 4699–4709.

[27] F.-L. Ng, M. M. Jaafar, S.-M. Phang, Z. Chan, N. A. Salleh, S. Z. Azmi, K. Yunus, A. C. Fisher, V. Periasamy, Reduced graphene oxide anodes for potential application in algae biophotovoltaic platforms, Scientific reports 4 (2014) 7562.

[28] L. Zhuang, Y. Yuan, G. Yang, S. Zhou, In situ formation of graphene/biofilm composites for enhanced oxygen reduction in biocathode microbial fuel cells, Electrochemistry Communications 21 (2012) 69–72.

[29] Y. Yuan, S. Zhou, B. Zhao, L. Zhuang, Y. Wang, Microbially-reduced graphene scaffolds to facilitate extracellular electron transfer in microbial fuel cells, Bioresource technology 116 (2012) 453–458.

[30] Y.-C. Yong, Y.-Y. Yu, X. Zhang, H. Song, Highly active bidirectional electron transfer by a self-assembled electroactive reduced-graphene-oxide-hybridized biofilm, Angewandte Chemie International Edition 53 (17) (2014) 4480–4483.

[31] J. Liu, Y. Qiao, C. X. Guo, S. Lim, H. Song, C. M. Li, Graphene/carbon cloth anode for high-performance mediatorless microbial fuel cells, Bioresource technology 114 (2012) 275–280.

[32] C. Richard, F. Balavoine, P. Schultz, T. W. Ebbesen, C. Mioskowski, Supramolecular self-assembly of lipid derivatives on carbon nanotubes, Science 300 (5620) (2003) 775–778.

[33] R. Frost, G. E. Jonsson, D. Chakarov, S. Svedhem, B. Kasemo, Graphene oxide and lipid membranes: interactions and nanocomposite structures, Nano letters 12 (7) (2012) 3356–3362.

[34] P. K. Ang, M. Jaiswal, C. H. Y. X. Lim, Y. Wang, J. Sankaran, A. Li, C. T. Lim, T. Wohland, O. Barbaros, K. P. Loh, A bioelectronic platform using a graphene-lipid bilayer interface, ACS nano 4 (12) (2010) 7387–7394.

[35] M. Hirtz, A. Oikonomou, T. Georgiou, H. Fuchs, A. Vijayaraghavan, Multiplexed biomimetic lipid membranes on graphene by dip-pen nanolithography, Nature communications 4.

[36] V. C. Sanchez, A. Jachak, R. H. Hurt, A. B. Kane, Biological interactions of graphene-family nanomaterials: an interdisciplinary review, Chemical research in toxicology 25 (1) (2011) 15–34.

[37] A. V. Titov, P. Král, R. Pearson, Sandwiched graphene-membrane superstructures, ACS nano 4 (1) (2009) 229–234.

[38] O. Parlak, A. P. Turner, A. Tiwari, On/off-switchable zipper-like bioelectronics on a graphene interface, Advanced Materials 26 (3) (2014) 482–486.

[39] A. B. A. B. A. D. S. C. Sanhita Ray, Sayantani Sen, A. Dasgupta,

[40] H. Li, R. Bashir, Dielectrophoretic separation and manipulation of live and heat-treated cells of listeria on microfabricated devices with interdigitated electrodes, Sensors and Actuators B: Chemical 86 (2) (2002) 215–221.

[41] J. H. Merritt, D. E. Kadouri, G. A. O'Toole, Growing and analyzing static biofilms, Current protocols in microbiology (2005) 1B–1.

[42] Dropsens,

[43] T. R. Garrett, M. Bhakoo, Z. Zhang, Bacterial adhesion and biofilms on surfaces, Progress in Natural Science 18 (9) (2008) 1049 – 1056.

[44] M. E. Davey, N. C. Caiazza, G. A. O'Toole, Rhamnolipid surfactant production affects biofilm architecture in pseudomonas aeruginosa pao1, Journal of bacteriology 185 (3) (2003) 1027–1036.

[45] A. Trapalis, N. Todorova, T. Giannakopoulou, N. Boukos, T. Speliotis, D. Dimotikali, J. Yu, Tio 2/graphene composite photocatalysts for nox removal: A comparison of surfactant-stabilized graphene and reduced graphene oxide, Applied Catalysis B: Environmental 180 (2016) 637–647.

[46] L. G. Cancado, A. Jorio, E. M. Ferreira, F. Stavale, C. Achete, R. Capaz, M. Moutinho, A. Lombardo, T. Kulmala, A. Ferrari, Quantifying defects in graphene via raman spectroscopy at different excitation energies, Nano letters 11 (8) (2011) 3190–3196.

[47] S. Eigler, C. Dotzer, A. Hirsch, Visualization of defect densities in reduced graphene oxide, Carbon 50 (10) (2012) 3666–3673.

[48] S. B. Grimm, M. Schweiger, S. Eigler, J. Zaumseil, High-

quality reduced graphene oxide by cvd-assisted annealing, The Journal of Physical Chemistry C, 120 (5)(2016), 3036–3041.

[49] S. Mao, G. Lu, K. Yu, Z. Bo, J. Chen, Specific protein detection using thermally reduced graphene oxide sheet decorated with gold nanoparticle-antibody conjugates, Advanced materials 22 (32) (2010) 3521–3526.

[50] A. Kaniyoor, S. Ramaprabhu, A raman spectroscopic investigation of graphite oxide derived graphene, AIP Advances 2 (3) (2012) 032183.

[51] J. Svensson, E. E. B. Campbell,Schottky barriers in carbon nanotube-metal contacts, Journal of Applied Physics 110 (11) (2011) 111101

[52] A. I. Ilin, L. I. Aparshina, S. V. Dubonos, B. N. Tolkunov, conduction electrons on the current–voltage characteristics of thin-film (2001) 17–21.

[53] P. Poncharal, C. Berger, Y. Yi, Z. Wang, W. A. de Heer, Room temperature ballistic conduction in carbon nanotubes, arXiv preprint cond-mat/0211515.

[54] B. S. Berlett, R. L. Levine, E. R. Stadtman, Use of isosbestic point wavelength shifts to estimate the fraction of a precursor that is converted to a given product, Analytical biochemistry 287 (2) (2000) 329–333.

[55] R. Kempaiah, S. Salgado, W. L. Chung, V. Maheshwari, Graphene as membrane for encapsulation of yeast cells: protective and electrically conducting, Chem. Commun. 47 (41) (2011) 11480–11482.

[56] G. Timp, Nanotechnology, 1999, Springer, New York.

[57] M. Dresselhaus, G. Dresselhaus, R. Saito, Carbon fibers based on c 60 and their symmetry, Physical Review B 45 (11) (1992) 6234.

Appendix A: Appendixes

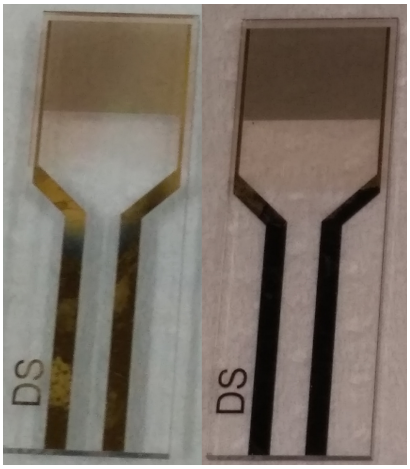

FIG. 10: *

Figure S1. Photographs of IDEs with biofilm grown on surface. Left: assymetric growth for g2 and right: uniform biofilm growth for control biofilm

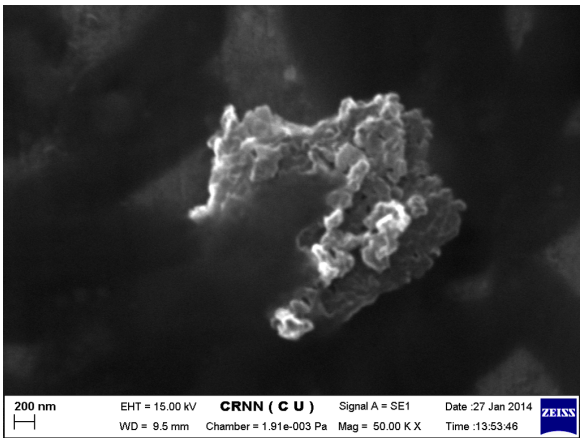

FIG. 11: *

Figure S2. High magnification SEM image showing wrinkled surface of graphene platelet (bright) trapped by biofilm cells(dark shadows). Image obtained without gold sputtering and composite grown on aluminium foil. Trapped platelets are on average 2 micron in diameter.

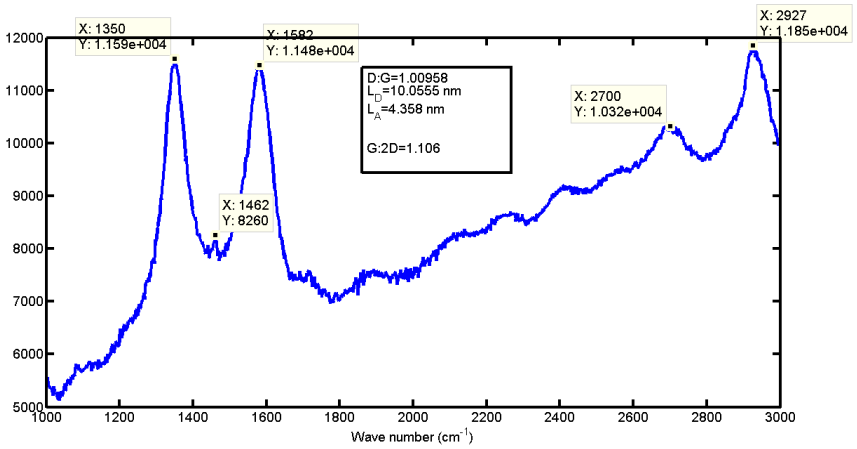

FIG. 12: *

Figure S3. Raman spectra of graphene sample dispersed in tetrahydrofuran and deposited on silicon wafer, obtained with 488 nm laser. Samples were microwaved for 90 s after deposition and $I_D : I_G$ ratio for these samples was found to be 1.00958. This ratio gave L_D=10.0055 nm but fitting to Tunistra-Koenig gave $L_A = 4$ nm. This is only possible with wrinkling/folding of graphene flakes. Peak at 2927 nm was a second harmonic of the one at 1462 nm, which is one of the several defect related peaks (D") that have been previously reported. Both presence of D" and a reduced L_D of 10.055 nm, compared to chloroform dispersed samples point towards extensive microwaving having induced defects into the sample.

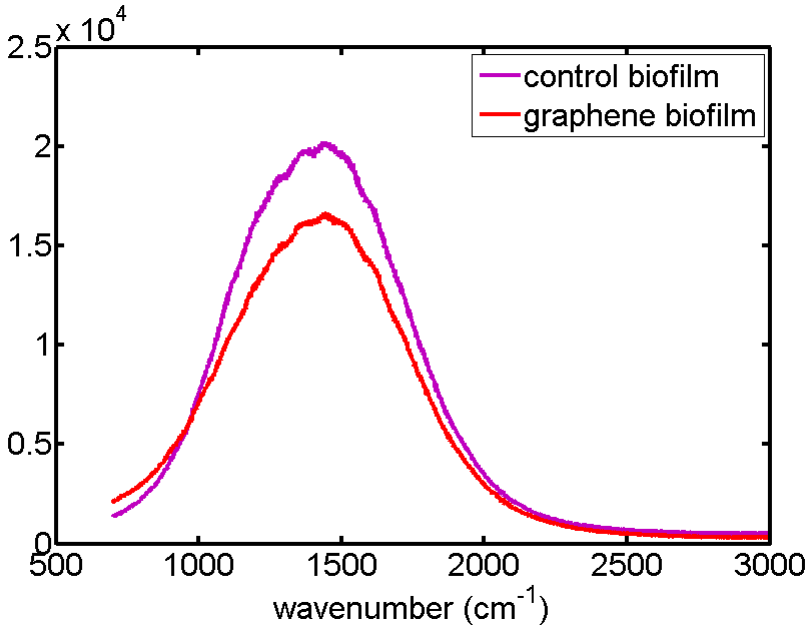

FIG. 13: *

Figure S4. Raman spectra obtained with dried control biofilm and graphene incorporated biofilm on 5th day of growth. Composites were grown on quartz pieces and spectra were obtained with 632 nm laser.

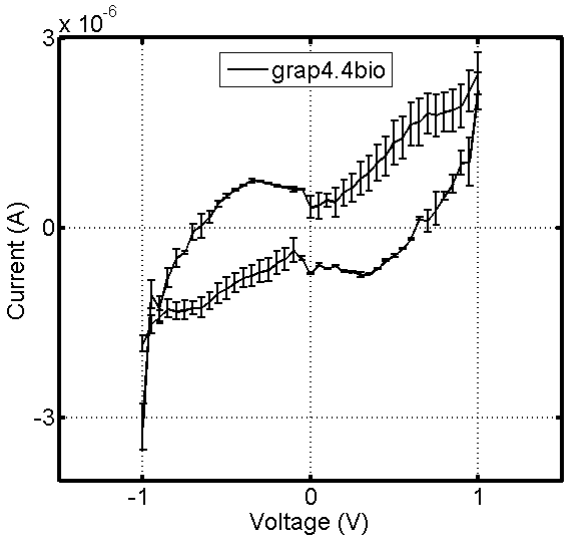

FIG. 14: *

Figure S5. Small voltage range IV curve for graphene-biofilm composite with IDE2.

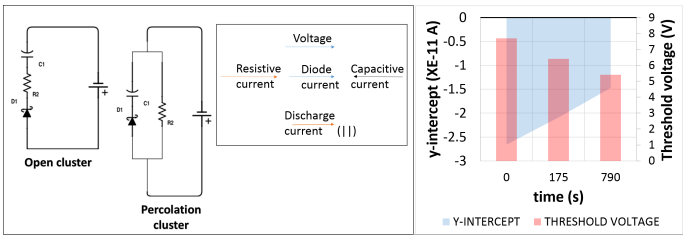

FIG. 15: *

Figure S6. (a) Open cluster may describe behaviour of the bio-composite material for lower dose of graphene than used for this work, when charge storage (as given by capacitive current) is not countered by flow of dissipative current in the direction opposite to applied voltage, i.e. no parallel path exists. Percolation cluster describes our case where there is an alternative, parallel pathway of current conduction that bypasses the capacitive circuitry, hence capable of dissipating most stored charge. (b) Capacitor current, given by y-intercept of consecutively run I-V measurements, as a function of time (measurement start) decreases with time. Threshold voltage for current conduction (for the same runs) as function of time. Threshold voltage decreases as capacitor current decreases (i.e. becomes less negative).